Study of the oscillatory flow of a yield-stress fluid in a cylindrical pipe

Author: Sebastián Alvariza Trinidad
Facultat de Física, Universitat de Barcelona, Diagonal 645, 08028 Barcelona, Spain.

Advisor: Ramón Planet & Jordi Ortín
(Dated: June 15, 2023)

Abstract: During this work we studied the oscillatory pipe flow of a Carbopol mixture. The velocity profiles show the non-linearity of the shear stress and the shear rate relation. For low frequencies the viscosity is high and the flow is plug-like. On the contrary, for high frequencies the force made by the piston is high enough to lower the viscosity value and induce a viscous fluid behaviour, leading to a Poiseuille-like profile. We also studied the rheological properties of samples of different concentrations and estimated the value of the yield stress, the consistency index and the flow index fitting the flow ramps to a Herschel-Bulkley-type equation.

I. INTRODUCTION

Non-Newtonian fluids find extensive applications in numerous fields and industries worldwide, such as food industry, cosmetics, and automotive. These fluids display interesting properties such as shear-thinning (a viscosity that decreases with the shear-rate), elasticity or the existence of minimum yield stress to flow, that are of great interest both from a technological and a fundamental point of view [1].

The relation between the shear rate, $\dot{\gamma}$, and the shear stress, σ, is commonly used to classify substances. For ordinary Newtonian fluids this relation is linear $\sigma = \eta\dot{\gamma}$ with η, the viscosity, constant. On the contrary, non-Newtonian fluids show various responses: the relation between σ and $\dot{\gamma}$ becomes non-linear in the case of shear-thinning fluids [2], σ can depend both with $\dot{\gamma}$ and γ in viscoelastic fluids [3], or the fluid needs a minimum yield stress to flow in yield-stress fluids $\sigma > \sigma_y$ [4].

Bingham pseudo-plastic fluids are shear-thinning fluids but also exhibit a yield stress that acts as a threshold that separates two different states. This behaviour can be described with the Herschel-Bulkley model [5]:

$$\begin{cases} \dot{\gamma} = 0, & \sigma < \sigma_y \\ \sigma = \sigma_y + \tilde{\eta}\dot{\gamma}^n, & \sigma \geq \sigma_y \end{cases} \tag{1}$$

where σ_y is the yield stress, $\tilde{\eta}$ the consistency index and n the flow index. For shear-thinning materials $n < 1$. From the model we see that under low stress these fluids behave as solids, while under high stress as viscous fluids. Mayonnaise, hair grease and mud are quotidian examples of yield-stress fluids.

Carbopol is the standard example of yield-stress fluids [4, 6]. It is a polymer frequently used as a thickening agent in gels, creams, lotions, pharmaceutical products, home care and industrial products, among many others. It consists of synthetic polymers, with each primary polymer being about 0.2 to 6.0 µm average diameter [6]. When a strong base is added to a solution of Carbopol and water it increases the pH, leading to chemical reactions that make the polymer swell as it absorbs water. The swelling and jamming of the polymers is what causes the gelification of the solution. Thus one can deduce that very low concentrations of carbomer will just lead to dense liquids. However, if the concentration is high enough, Carbopol microgels swell and start interacting with each other and undergoing a jamming transition [7].

Our main goal here is to study the oscillatory flow of a Carbopol solution in a cylindrical pipe. Oscillatory pipe flows are present in the respiratory and circulatory systems of living beings [8], industrial processes and acoustics [3]. We will force the fluid flow using a piston at the lower part of the vertical pipe and obtain the flow velocity profiles for different frequencies and amplitudes of oscillation.

II. INSTRUMENTATION AND METHODOLOGY

A. Sample preparation

The samples used in both the rheology and the tube experiment were made using Lubrizol's Carbopol. We first dissolved the carbomer in distilled water at room temperature using a magnetic stirrer. Then we store the samples for 2 to 5 days to get rid of a frost layer sitting on top of the samples and air bubbles present in the bulk phase. Finally we introduced 3 mL of sodium hydroxide as the base agent to trigger gelation and shook up all of the samples to ensure the NaOH was well distributed so we obtained an homogeneous gel.

Five samples were made for the rheological caracherization of Carbopol gels with concentrations 2.0 wt%, 1.5 wt%, 1.0 wt% and 0.5 wt%. Samples with Carbopol concentrations ≤ 0.25 wt% did not gel as the concentration was not enough to undergo the jamming transition. For the main experiment we made 1 L of solution of 1 wt% concentration following the same steps (introducing 60 mL of NaOH this time) but we added polyamide particles to the solution before mixing it. These particles are tracers used to perform the particle image velocimetry

Concentration (wt%)	σ_y (Pa)	$\tilde{\eta}$ (Pa·s^n)	n
0.5	44.626	22.136	0.50
1.0	99.607	32.888	0.48
1.0 (postmortem)	94.335	32.551	0.48
1.5	329.135	69.244	0.41
2.0	436.13	50.874	0.53

TABLE I: Rheological parameters of the different samples studied obtained by fitting the Herschel-Bulkley model.

(PIV, see Sec. II D). To gel the sample we first put it inside the cylindrical pipe used in the main experiment and then with a funnel and a small tube we introduced the NaOH from the bottom to the top. This was made in an attempt to obtain an homogeneous gel inside the tube. Due to the nature of the gellation process air bubbles appeared in the bulk of the final fluid and remained trapped, as the buoyant force was not strong enough to surpass the yield stress.

B. Rheological characterization of Carbopol

To characterize the rheological properties of the Carbopol solutions we used a *Discovery HR 20* rheometer from *TA Instruments* with a plate-plate geometry of 40 mm diameter and a gap space of 10^3 µm to avoid polyamide particles to jam inside the rheometer. To prevent the samples from slipping, sandpaper was placed on both the geometry and the plate surfaces, as slipping would lead to inaccurate results.

We first made a flow ramp applying a decreasing shear rate over time to obtain the shear stress and the viscosity. Slipping phenomena would appear in the case of an increasing shear rate, resulting in invalid measurements [5]. Second, to characterize the temporal response of the Carbopol gels we obtain the storage modulus and the loss modulus as a function of the angular frequency by performing an oscillatory test. Instead of rotating in a single direction, the geometry oscillates around the rotation axis between two given amplitudes increasing the frequency over time. We did this test at controlled stress, so that the amplitude of the oscillation correspond to a stress value. After this procedure, a second flow ramp was made to ensure the samples were not damaged during the oscillatory test.

We have repeated the rheological tests on the sample used in the oscillatory pipe flow before and after the experiment, to track any possible changes in the fluid due the experimental protocol itself or by the possible aging of the material. Figure 1 shows the flow ramp for both tests in blue for the original sample and in red for the postmortem sample. No significant changes are identified.

Figure 1 top panel shows the flow ramps for the different samples. We clearly observe a non-zero yield-stress value at lower $\dot{\gamma}$ and a shear-thinning behaviour at larger

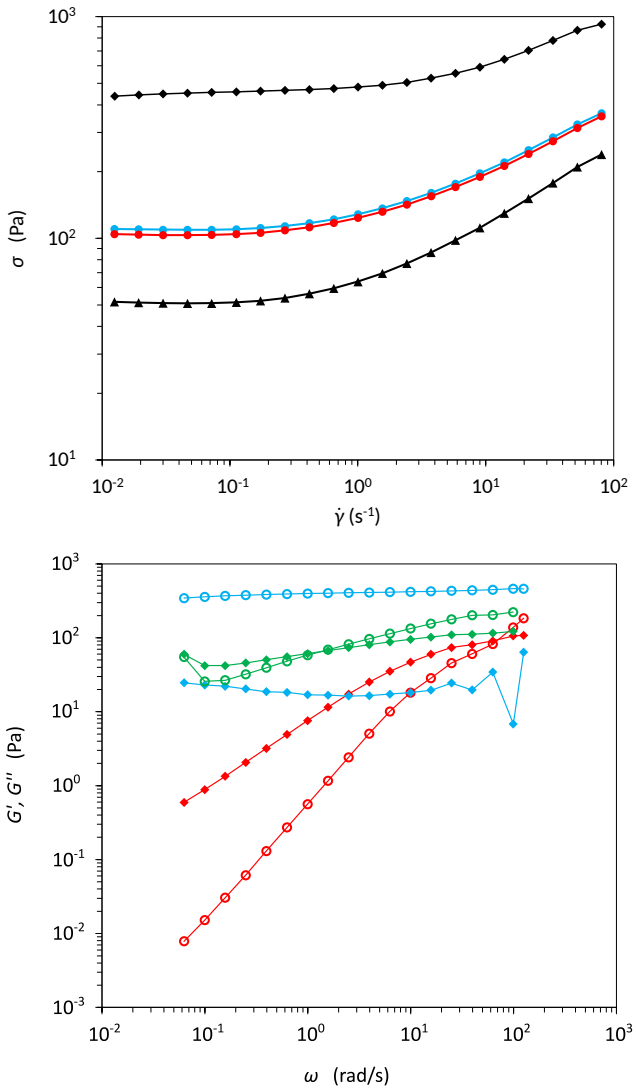

FIG. 1: TOP panel: shear stress as a function of the shear rate for four samples: 0.5 wt% (triangles), 1.0 wt% (blue circles), 1.0 wt% postmortem sample (red circles), and 2.0 wt% (diamond). BOTTOM panel: the storage modulus (dots) and the storage modulus (diamonds) vs oscillation frequency. Colors represent the different stresses applied: $\sigma_b = 10$ Pa (blue), $\sigma_g = 160$ Pa (green), and $\sigma_r = 320$ Pa (red).

shear rates. This causes the viscosity to slowly decrease as the shear rate increases once the yield stress is surpassed. Fitting the curves to a Herschel-Bulkley-type equation 1 we can estimate the yield stress and the consistency and flow index. Those values are collected in Table I.

In the bottom panel of Fig. 1 we show the results for the storage G' and loss G'' modulus for the 1 wt% sample at different stress amplitudes. For low stress amplitudes the storage modulus is of greater value than the loss modulus and both are almost constant. This is typically observed in gels with solid-like behaviors. Otherwise, for high stress it is the other way around,

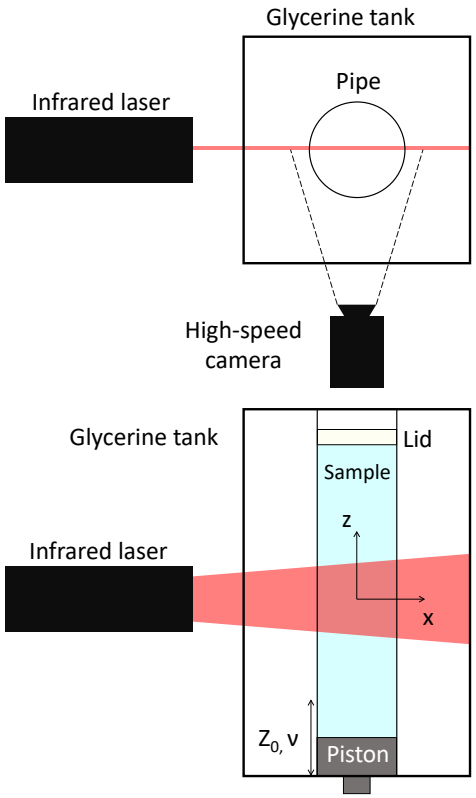

FIG. 2: Sketch of the experimental setup. Top and lateral views of the setup.

$G'' \gg G'$ and an increase of both modulus with ω is observed. This response is typical of liquid-like fluids. When the stress takes an intermediate value the storage modulus is larger than the loss modulus for lower frequencies and there is a crossover after which the loss modulus stays larger than the storage modulus.

C. Experimental setup

The experimental setup is composed of a methacrylate tube of 50 mm inner diameter ($r_0 = 25$ mm), 60 cm length and 5 mm thick that contains the solution. The whole tube is surrounded by a rectangular methacrylate case filled with glycerin. This serves the purpose of reducing the optical aberration due to the circular shape of the pipe, since methacrylate and glycerine have approximately the same refractive index. A Teflon piston located at the lower end of the tube to impose the oscillatory motion and we also placed a freely moving plastic lid at the surface of the fluid to avoid free interface effects that might interfere with the flow in the bulk [3]. An infrared laser and a high-speed camera are placed as shown in Fig. 2 to record the images to later perform the PIV analysis (see Sec. II D). The laser is connected to the camera and it only activates when the camera shutter is open.

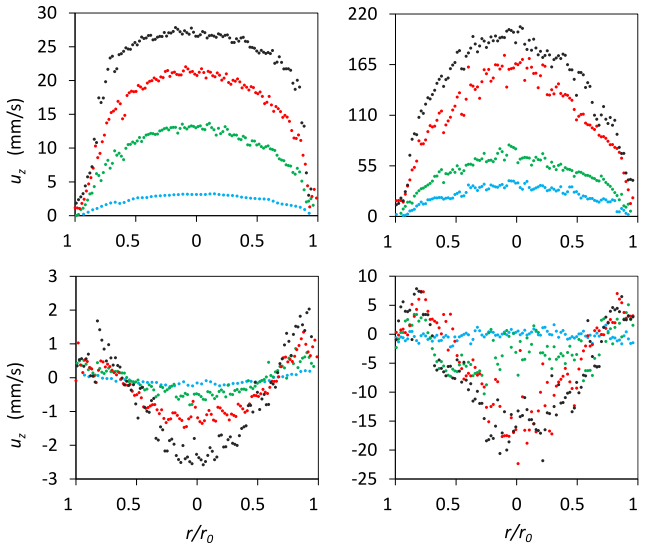

FIG. 3: Vertical velocity maps. TOP panels correspond to $\nu = 0.6$ Hz (LEFT) and $\nu = 3.6$ Hz (RIGHT) for $\omega_0 t = 0$. BOTTOM panels corresponds to the velocity profiles with $\omega_0 t = \pi/2$. The color code indicate the amplitude of the piston: $z_0 = 0.75$ mm (blue), $z_0 = 1.99$ mm (green), $z_0 = 3.29$ mm (red) and $z_0 = 4.62$ mm (black).

With this setup we could control both the frequency ν and the amplitude z_0 of the piston oscillations. Connected to the piston there is a Linear Variable Differential Transformer (LVDT) with a resolution of 0.03 mm, that allows us to record the vertical position of the piston in time [3].

D. Image acquisition and PIV

Images were taken in a dark room to avoid light reflexes in the tube. As mentioned earlier, the camera shutter triggers the laser, which highlights the polyamide particles. At the same time we record the amplitude of the piston's oscillations with the LVDT, the camera sends a signal when the shutter opens, allowing us to relate each image with the corresponding piston phase.

The image analysis was performed with the particle image velocimetry technique [9], using PIVlab, a graphical user interface based PIV free software developed in MATLAB [10]. The program allowed us to both extract the velocity field using image pairs and analyze them within the same environment.

III. RESULTS

Figure 3 shows the velocity profiles for different frequencies and amplitudes, both at $\omega_0 t = 0$ (Fig. 3 top panels) and $\omega_0 t = \pi/2$ (Fig. 3 bottom panels). Phase

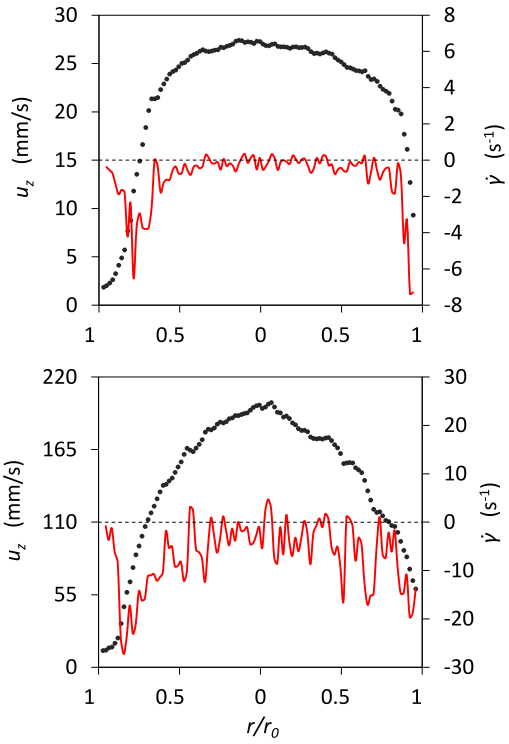

FIG. 4: Smoothed velocity profile and shear rate along the r axis, both for $\omega t = 0$. TOP panel shows $\nu = 0.6$ Hz. For the BOTTOM panel $\nu = 3.6$ Hz. The amplitude is $z_0 = 4.6$ mm for both.

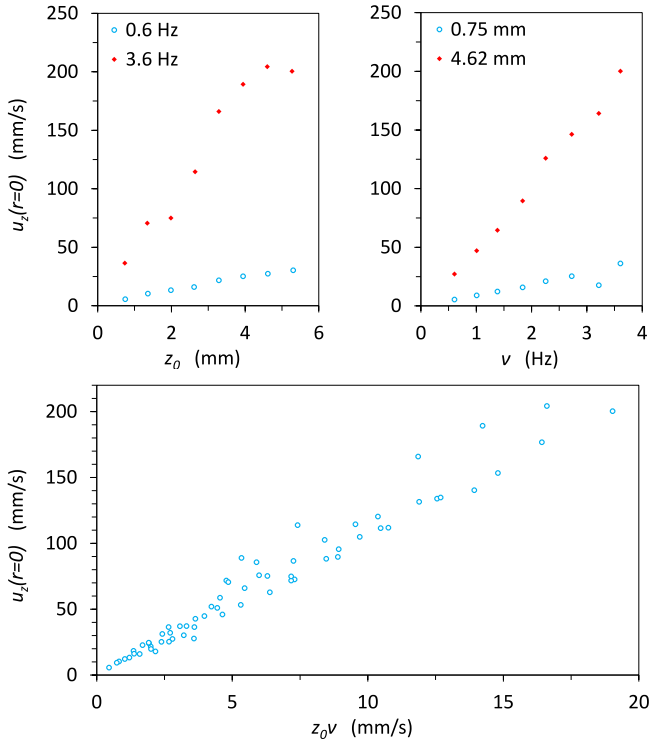

FIG. 5: Velocity at the center of the tube at $\omega_0 t = 0$ vs amplitude keeping ν constant (TOP LEFT) and vs amplitude keeping z_0 constant (TOP RIGHT). BOTTOM figure shows the product $u_z(r = 0)$ vs $z_0\nu$.

$\omega_0 t = 0$ meaning the moment where the speed of the piston is at its maximum and $\omega_0 t = \pi/2$ at its minimum.

From Fig. 3 top panel we see that for low frequencies the velocity profile is close to 0 at the pipe walls and rises abruptly to form a plateau region. This effect is better appreciated at higher amplitudes, at which the profile shows a plug flow. Alternatively, at higher frequencies we observe a parabolic profile, indicating that the flow is Poiseuille-like (as expected for a Newtonian fluid).

For $\omega t = \pi/2$ the velocity remains close to 0 for low amplitudes. At higher amplitudes the velocity reaches a maximum value in the center of the pipe and has two smaller peaks close to the walls.

Finally, we can also notice how at higher frequencies there's a considerable amount of noise compared to the lower ones. This may be caused by the bubbles contained in the tube.

IV. DISCUSSION

We observed plug flow velocity profiles for the low frequency experiments shown in Fig. 3, meaning that the bulk of the fluid reacts to the forcing exerted by the piston as a "rigid body". Plug flows are characterized by flat velocity profiles that rapidly decays at the walls to fulfill continuity ($u_z = 0$ at the walls), as we see in Fig. 3 for low frequencies. Plug flows are also typically observed in ideal liquids ($\eta \to 0$) which is clearly not our case. This indicates that under these circumstances the shear stresses are localized close to the walls and are strong enough to surpass the yield stress but not to fluidize the whole volume of the yield-stress fluid. Top panel in Fig. 4 shows the shear-rate ($\dot{\gamma} = du_z/dr$) corresponding to one of these cases and it is possible to see how the shear is localized close to the walls. Alternatively, at higher frequencies and $\omega_0 t = 0$ (see Fig. 3 right panels) the flow is Poiseuille-like, dropping to 0 at the walls caused by the non-slip conditions and reaching a maximum value at the center of the tube. This velocity profile is that of a viscous fluid, so the whole volume of fluid has overcome the yield stress value and flows (see Fig. 4 bottom panel where now γ changes continuously in opposition to what we observed for low frequency forcing). Figure 4 clearly shows the difference of the shear rate tendency in both cases, reinforcing the idea that the sample behaves differently in lower frequencies than how it does at higher frequencies.

The fact that shear rates are non-zero for large forcing experiments is consistent with the rheology of Carbopol, since for large enough stresses Carbopol flows as a liquid (see Fig. 1). Same reasoning can be done for the low frequency experiments (lower forcing experiments) where the shear stress is not strong enough to overcome the

yield stress and therefore Carbopol behaves as a solid on those parts.

We also show in Fig. 5 the velocity at the center of the pipe at $\omega_0 t = 0$. Top panels in Fig. 5 display $u_z(r = 0)$ as a function of the applied frequency at constant amplitude, and as a function of amplitude for a given frequency. Finally in the bottom panel of Fig. 5 we plot the velocity as a function of the piston velocity $z_0\nu$ and we clearly see that $u_z(r = 0) \propto z_0\nu$. This proportionality is expected for Newtonian but still holds in the present case.

Finally, the fluid velocity profiles shown in Fig. 3 are comparable to those observed in Newtonian fluids. Plug flow profiles in Newtonian fluids are observed in oscillatory pipe flows when the Stoke's parameter $\Lambda = r_0\sqrt{\rho\omega_0/(2\eta)}$ is much lager than 1, and parabolic profiles appear when $\Lambda < 1$ [3]. In the present case of Carbopol, the viscosity thins with the shear-rate, so larger $\dot{\gamma}$ results in lower viscosity. Then experiments with lower ω_0 should result in Stokes parameters lower than for those experiments at larger ω_0. Therefore the transition from a plug flow towards a parabolic Poiseuille flow seems reversed in the case of this yield-stress fluid.

V. CONCLUSIONS

- The fluid behaves as a Bingham pseudo-plastic, as the flow curve shows a shear-thinning behaviour for all concentrations. This is reassured by the values of the flow index estimated by fitting the data to the Herschel-Bulkley model.

- The oscillatory experiments allow us to see that for $\sigma = 10$ Pa Carbopol gel at 1 wt% behaves as a solidgel, as the storage modulus is considerably larger than the loss modulus. At $\sigma = 160$ Pa the higher stress cause a non-linear response and both magnitudes cross each other. Finally, for $\sigma = 320$ Pa the solution is in fluid state, thus the loss modulus is much higher than the storage modulus.

- The plug flow observed in the velocity maps at $\omega_0 t = 0$ for low frequency is caused by the low pressure induced by the piston, There is no wall slip due to the viscosity of the sample.

- On the contrary, the high frequency profiles indicate a viscous fluid behaviour. The viscosity of the fluid drops due to the higher pressure made by the piston, which induces a Poiseuille-like flow in the pipe.

Acknowledgments

I really want to thank Dr. R. Planet for the guidance and help he provided me during the realization of this work, my family for always rooting for me and all the people that made this project possible, both in a direct and indirect way, I'm really thankful for having their support and help.

[1] Patrick Oswald, *Rheophysics The Deformation and Flow of Matter* (Cambridge University Press, 2009).
[2] Daniel Arrufat. "Oscillatory pipe flow of aqueous xanthan gum solutions". Undergraduate thesis, Universitat de Barcelona (2019).
[3] Laura Casanellas. "Oscillatory pipe flow of wormlike micellar solutions". PhD Thesis, Universitat de Barcelona (2013).
[4] Daniel Bonn, Morton M. Denn, Ludovic Berthier, Thibaut Divoux, and Sébastien Manneville. "Yield stress materials in soft condensed matter". Rev. Mod. Phys. **89**: 035005 (2017).
[5] Thibaut Divoux, Catherine Barentin and Sébastien Manneville. "From stress-induced fluidization processes to Herschel-Bulkley behaviour in simple yield stress fluids". Soft Matter **18**: 8409-8418 (2011).
[6] E. Di Giuseppe, F. Corbi, F. Funiciello, A. Massmeyer, T.N. Santimano, M. Rosenau, A. Davaille. "Characterization of Carbopol® hydrogel rheology for experimental tectonics and geodynamics". Tectonophysics **642**: 29-45 (2015).
[7] F. K. Oppong · J. R. de Bruyn. "Mircorheology and jamming in a yield-stress fluid". Rheological Acta **50**: 317–326 (2011).
[8] Ortín J. "Stokes layers in oscillatory flows of viscoelastic fluids". Phil. Trans. R. Soc. A **378**: 20190521 (2019).
[9] Markus Raffel, Christian E. Willert, Steve T. Wereley and Jürgen Kompenhans, *Particle Image Velocimetry. A Practical Guide*, (Springer, Berlin 2007, 2nd ed.).
[10] Thielicke, William and René Sonntag. "Particle Image Velocimetry for MATLAB: Accuracy and Enhanced Algorithms in PIVlab." Journal of Open Research Software **9**: 12 (2021).